

Polymer dynamics: from synthetic polymers to proteins

Dieter Richter

Research Center Juelich, Germany. Correspondence e-mail: d.richter@fz-juelich.de

In polymeric materials, the structures, the macroscopic mechanical and rheological properties, and the phase changes are determined to a high degree by thermal motion of the atoms and molecules. Most of the relevant dynamics take place on mesoscopic lengths and timescales in between the picosecond atomic scale and the macroscopic frame. Offering the proper space–time observation window, neutron spin echo spectroscopy uniquely addresses these motions. We briefly present some key experimental results on the mesoscopic dynamics of polymer systems. We address briefly the standard model of polymer motion, the Rouse model, the role of topological confinement as expressed in the reptation model and, finally, processes limiting the confinement – we discuss contour length fluctuations and constraint release of entangled chains. Very recently it also became possible to directly identify large-scale internal dynamics of proteins by neutron spin echo. We report the results of these pioneering studies, which are most likely to initiate further experiments on the large-scale motions of proteins and their relation to protein function.

© 2007 International Union of Crystallography
Printed in Singapore – all rights reserved

1. Introduction

Neutron spin echo (NSE) spectroscopy, the highest resolution neutron technique, provides a time resolution in the 100 ns range enabling access to molecular motion on a mesoscopic timescale between the atomic picosecond scale and macroscopic times. At this scale, the molecular motions of polymers that underlie their macroscopic viscoelastic behaviour take place. Large-scale domain motions of biomolecules which may be important for their function take place in similar space–time frames.

The dynamics of long-chain flexible polymers constitute fascinating physics and at the same time represent one of the great challenges of modern material science (Richter *et al.*, 2005). The drive towards a molecular understanding of the complex viscoelastic properties of polymer liquids is a focal point of rheology and connects the classical chemical engineering approach with modern physics. In this context, the tube model invented by de Gennes (1971) and Doi & Edwards (1978) has proven to be the most successful molecular model describing the topological confinement enacted by the mutually interpenetrating polymer chains in the melt. The model is based on the idea that large-scale transversal chain motion is suppressed by topological constraints imposed by neighbouring chains. Chain dynamics are restricted to a snake-like motion within a virtual tube following the coarse-grained chain contour. In terms of this reptation model, a theory of viscoelasticity has been developed that describes the main features of polymer melt rheology.

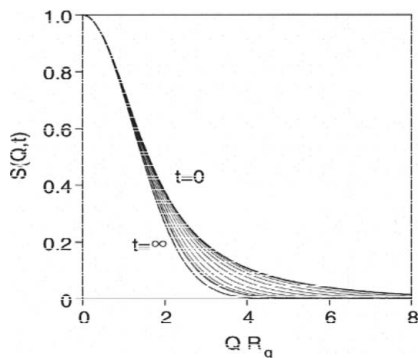
Protein domain motions, on the other hand, are critical for proteins to coordinate precise biological functions. For example, coupled domain motions occur in genome regulatory proteins, motor proteins, signalling proteins and structural proteins. Structural studies have documented the conformational flexibility in proteins accompanying their activity. Results for macroscopic studies such as biochemical kinetics and single-molecule-detection studies have also shown the importance of conformational dynamics and Brownian thermal

fluctuations within the proteins. However, the time-dependent dynamic processes that facilitate protein domain rearrangements remain poorly understood and experimentally nearly untouched (Bu *et al.*, 2005).

2. Neutron spin echo as quasielastic small-angle neutron scattering (Mezei, 1980)

The inelastic analysis of small-angle neutron scattering (SANS) comprises most of the NSE investigations on polymeric systems. This automatically means that the scattering intensity is usually dominated by coherent scattering, which is favourable for conventional NSE techniques. NSE is usually performed on deuterated materials containing ‘labelled’ protonated components. The resulting contrast of scattering length density compared to the hydrogenated objects to be observed gives rise to a considerable coherent SANS intensity. For larger scattering vectors ($Q > 2\text{--}5\text{ nm}^{-1}$) incoherent scattering becomes more and more important. Considering the coherent scattering, only the NSE intensity $S(Q, t=0)$ directly relates to the SANS intensity $S(Q)$. In a coarse analogy, the SANS intensity corresponds to the scattering of a frozen configuration of the scattering objects (a ‘snapshot’), whereas after a time t some objects have moved, causing – on average – a more and more blurred configuration, the scattering of which corresponds to $S(Q, t)$. Since sharp edges and fine structures are blurred first, the high Q parts of $S(Q, t)$ decay faster.

As an example we consider the Rouse dynamics of a polymer chain in the melt. The Rouse model treats the dynamics of a Gaussian chain in a heat bath. Thereby it implicitly assumes that on the lengths and timescales considered all forces from local potentials which are related to the individual chemical nature of a given polymer have already decayed. Then only entropic forces originating from the conformational chain entropy drive the dynamics. At scales $QR_E > 1$, where R_E is the chain end-to-end distance, the normalized single


Figure 1

Development of $S(Q, t)$ for Rouse motion for different times. Note that in addition to these intra-chain dynamics, the chain is subject to translational diffusion as a whole.

chain dynamic structure factor S for this model can be written as a function of a scaling variable $u = Q^2(W\ell^4 t)^{1/2}$ combining spatial and temporal scales,

$$S(u) = \int_0^\infty ds \exp \left\{ -s - (u/3\pi) \int_0^\infty [\cos(6xs/u)]/x^2 \times [1 - \exp(-x^2)] dx \right\}. \quad (1)$$

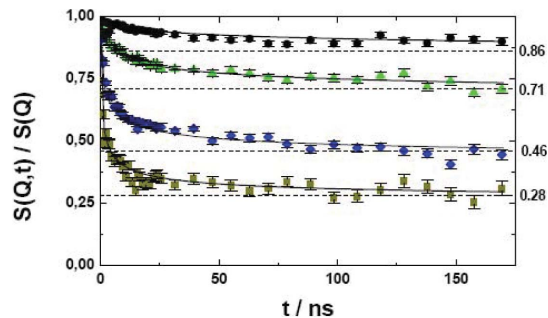
Thereby $W = 3k_B T / (\zeta \lambda^2)$ is the elementary Rouse frequency. It is given by the ratio of the entropic force $3k_B T / \lambda^2$ and the friction coefficient ζ . λ^2 is the mean squared segment length.

Equation (1) is only valid in the asymptotic Q^{-2} tail of the scattering function. A full treatment (de Gennes, 1967) yields the dynamic structure factor also in the low- Q limit. At $t = 0$ this immediately leads to the well known Debye function $S(Q) = N f_{\text{Debye}}(Q^2 R_g^2)$ with $f_{\text{Debye}}(x) = (2/x^2)[\exp(-x) - 1 + x]$. Fig. 1 displays the temporal evolution of the ‘quasielastic SANS’. The uppermost curve corresponds to the Debye function, while the lower curves visualize the decay of the structure factor due to the Rouse relaxation. For $t \Rightarrow \infty$ all internal chain correlations are lost and the structure factor nearly displays the Gaussian density profile within a polymer coil. We note that the polymer coil in addition to the Rouse modes is also the subject of translational diffusion.

3. Large-scale polymer dynamics – reptation and beyond

For long chains topological chain–chain interactions in terms of entanglements become important and dominate the dynamical behaviour. In the famous reptation model these constraints are described by a virtual tube which localizes a given chain and limits its motion to a one-dimensional Rouse motion inside the tube (local reptation) and a slow diffusive creep motion out of the tube (reptation) (de Gennes, 1971; Edwards & Grant, 1973). Applying NSE spectroscopy, it has become possible to observe the dynamic structure factor $S(Q, t)$ associated with tube confinement and local reptation.

de Gennes (1981) and Doi & Edwards (1978, 1986) have formulated a tractable analytic expression for the dynamic structure factor. Thereby they neglected the initial Rouse regime *i.e.*, the derived expression is valid for $t > \tau_e$ once confinement effects become important (τ_e is the entanglement time, the Rouse relaxation time of an entanglement strand). The dynamic structure factor is composed from two contributions, $S^{\text{loc}}(Q, t)$ and $S^{\text{esc}}(Q, t)$, reflecting local reptation and escape processes (creep motion) from the tube,


Figure 2

The dynamic structure factor from an $M_w = 36 \text{ kg mol}^{-1}$ PE melt at 509 K as a function of time. The solid lines are a fit with the reptation model [equation (2)]. The Q values are from the top $Q = 0.05, 0.077, 0.115$ and 0.145 \AA^{-1} . The horizontal dashed lines display the prediction of the Debye–Waller factor estimate for the confinement size (see text).

$$\frac{S_{\text{chain}}(Q, t)}{S_{\text{chain}}(Q)} = 1 - \exp\left(-\frac{Q^2 d^2}{36}\right) S^{\text{loc}}(Q, t) + \exp\left(-\frac{Q^2 d^2}{36}\right) S^{\text{esc}}(Q, t). \quad (2)$$

The local reptation part was calculated as

$$S^{\text{loc}}(Q, t) = \exp\left(\frac{t}{\tau_0}\right) \text{erfc}\left(\frac{t}{\tau_0}\right)^{1/2}, \quad (3)$$

where $\tau_0 = 36/(W\ell^4 Q^4)$.

For short times, $S_{\text{chain}}(Q, t)$ decays mainly due to local reptation [first term of equation (2)], while for longer times (and low Q) the second term resulting from the creep motion dominates. The ratio of the two relevant timescales τ_0 and τ_d is proportional to N^3 . Therefore, for long chains at intermediate times $\tau_e < t < \tau_d$ a pronounced plateau in $S_{\text{pair}}(Q, t)$ is predicted. Such a plateau is a signature for confined motion and is present also in other models for confined chain motion.

In Fig. 2 dynamic structure factor data from an $M_w = 36 \text{ kg mol}^{-1}$ polyethylene (PE) melt are displayed showing very clearly the tendency to form plateaux at high times (Richter *et al.*, 2005). In the spirit of equation (2) and neglecting the ongoing decay of $S_{\text{chain}}(Q, t)$ due to local reptation, from the heights of the plateaux achieved we may obtain a first estimate for the amount of confinement. Identifying the plateau levels with a Debye–Waller factor describing the confinement we get $d = 45 \text{ \AA}$, a value which is a lower estimate for the true tube diameter, since $S^{\text{loc}}(Q, t)$ is not fully relaxed. The horizontal dashed lines in Fig. 2 are the predictions from this Debye–Waller factor estimate.

While NSE experiments support the tube concept of topological confinement in long-chain polymer systems (Schleger *et al.*, 1998), a close comparison of linear rheology data with predictions of the tube model indicates the existence of additional processes that release the topological confinement (McLeish, 2002), such as fluctuating chain ends which escape the tube confinement (contour length fluctuations, CLFs) and the relaxation of the tube itself (constraint release, CR). While CLF is an effect of the confined chain itself, CR stems from the movement of the chains building the tube, which of course undergo the same dynamical processes as the confined chain. The CR process is schematically depicted in Fig. 3.

CLFs are a key mechanism for the relaxation at earlier times and also the basis for hierarchical relaxation processes of branched polymers, where CLFs are considered to be the fundamental process facilitating the release of side branches.

The CLF effect evolves from the participation of the chain ends in the local reptation process. Any chain retraction and subsequent

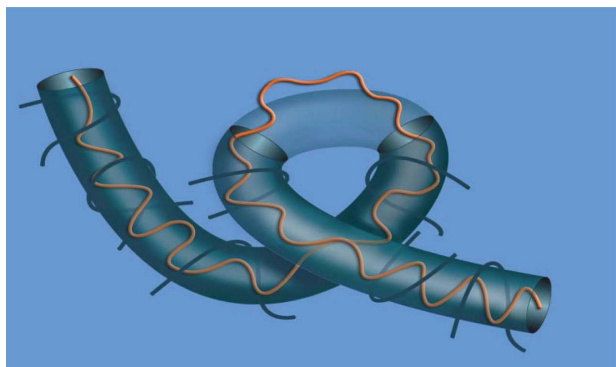


Figure 3
Schematic presentation of the CR mechanisms: the dissolving of entanglements allow chain motions beyond the initial tube constraints.

expansion will lead to a loss of memory of the original confinement of the tube. Thus, the tube becomes shorter with time. Mathematically the problem is treated as a first passage problem. Whenever a tube contour s is visited by the free end, it ceases to exist. The functional form of the tube survival probability $\mu(t)$ has been derived from scaling arguments, yielding (Likhtmann & McLeish, 2002)

$$\mu(t) = 1 - \left(\frac{C_\mu}{Z}\right) \left(\frac{t}{\tau_c}\right)^{1/4}, \quad (4)$$

where the numerical constant $C_\mu = 1.5 \pm 0.02$ is obtained from stochastic simulations, $Z = N/N_e$ is the number of entanglements and N_e is the number of segments forming an entanglement strand. Equation (4) provides quantitative knowledge about the chain fraction which at a time t is still confined. All parameters are known from NSE experiments on the dynamics of asymptotically long chains, where the CLF effect does not play a role.

With this knowledge, an experiment was designed in which the dynamic structure factor of a chain which is subject to CLF was compared with that of an identical chain where the contrast of those segments which are affected by CLF within the experimental time frame was matched. The experimental idea is displayed in Fig. 4. Case (a) is realised by performing an experiment on a fully protonated chain in a deuterated matrix. In this case the full chain dynamics including the CLFs are observed. Case (b) is realised by a chain in

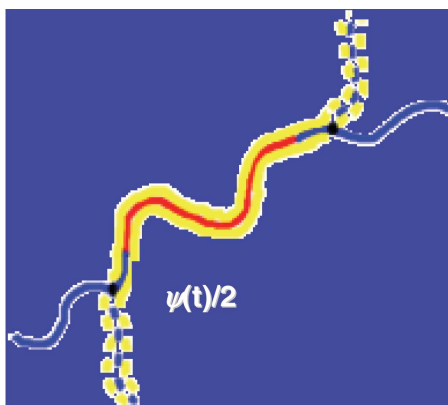


Figure 4
For a fully protonated chain in a deuterated matrix local reptation and contour length fluctuations are visible. For a centre-labelled (protonated) chain with deuterated chain ends in a deuterated matrix only local reptation is visible, the contour length fluctuations of the chain ends are masked. $\psi(t)/2$ denotes the time-dependent chain fraction release at one end.

which the inner part is protonated while the two outer chain sections of a length which would be affected by CLF are deuterated and thus are not visible in the deuterated matrix. Then the dynamics should be equal to those of an asymptotically long fully confined chain.

With the known parameters for PE, equation (4) calculates that on average on each side 220 monomers are released during the observation time of 190 ns. The contrasting experiments were performed on two different chains of molecular weight 25 kg mol^{-1} , one of which was fully hydrogenated and the other having deuterated labels of $M_w \simeq 4 \text{ kg mol}^{-1}$ corresponding to 260 monomers on each end. Both were studied in a deuterated matrix of the same molecular weight (Zamponi *et al.*, 2005).

In Fig. 5 the measured normalized dynamic structure factor $S(Q, t)/S(Q)$ is plotted as a function of time t for different Q values. For a better visibility not all Q values are shown. Fig. 5 presents the experimental results for the two chains. In all cases at short times a strong initial decay is observed which is due to the initial free Rouse motion. For longer times the decay is strongly reduced, transgressing into the confinement-related plateau behaviour. Comparing the levels of decay in Fig. 5 we realise that $S(Q, t)/S(Q)$ from the fully labelled chain decays significantly faster than that from the corresponding centre-labelled counterpart. The constraints are apparently stronger for the centre-labelled chain than for the chain where the ends are also visible. We also note that in the case where the ends were masked, the centre part of the chain shows exactly the same structure factor as a very long chain (Zamponi *et al.*, 2005), signifying directly the action of CLF at the chain ends and the remaining full confinement in the centre. The agreement of these two data sets also means that for the 25 kg mol^{-1} chain the effect of constraint release is indeed negligible.

We now discuss the other reptation limiting process, the constraint release. To separate the effect of CR from the CLF process, one has to consider a labelled chain which is long enough that end effects like CLF do not play a role ($M_w = 36 \text{ kg mol}^{-1}$). The CR effect is then studied in changing the molecular weight of the matrix chains over the range from 36 to 1 kg mol^{-1} . Comparing the dynamic structure factor of the long chain in successively shorter matrix chains, a clear transition from confined reptation-like motion in long matrix chains to free Rouse motion in short matrix chains is observed. This can be demonstrated well in a Rouse scaling representation [see equation (1)] of the dynamic structure factor (Fig. 6), where $S(Q, t)$ is plotted versus $(Q^2 W \ell^4 t)^{1/2}$. In this representation all $S(Q, t)$ need to collapse

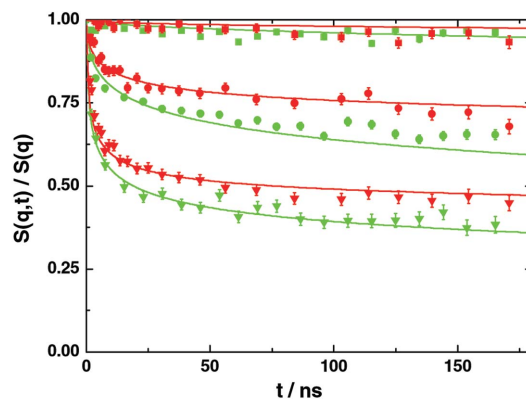


Figure 5
Dynamic structure factor of a centre-labelled 25 kg mol^{-1} PE chain (red symbols) compared to a fully labelled chain (green symbols) of the same overall molecular weight. Q values (in nm^{-1}): 0.5 (squares), 0.96 (circles), 1.15 (triangles). Lines: for centre-labelled chain, pure reptation model [equation (2), red]; for fully labelled 25 kg mol^{-1} chain (green) CLF was considered (see Lyamichev *et al.*, 1993).

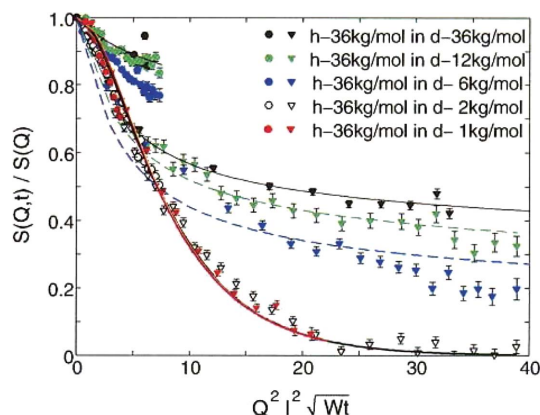


Figure 6

Dynamic structure factor of a long labelled chain ($M_w = 36 \text{ kg mol}^{-1}$) in different shorter matrix chains ($M_w = 36, 12, 6, 2$ and 1 kg mol^{-1} as indicated in the plot) in a Rouse scaling representation for two different Q values (circles 0.5 nm^{-1} , triangles 1.15 nm^{-1}). The lines correspond to fits with equation (2) (reptation) or equation (1) (Rouse), respectively.

into one master curve. On the other hand, if topological constraints are evident a length scale comes into play (in the reptation model the tube diameter) and such scaled dynamic structure factors split up for different Q values.

For the long chain in a matrix of the same molecular weight, a confinement as for infinitely long chains is observed. This means that for a 36 kg mol^{-1} chain neither CLF nor CR play a significant role in the accessible NSE time range, and the chain remains confined inside the tube. With decreasing matrix length (12 or 6 kg mol^{-1} ; Fig. 6) an increasing loss of confinement becomes visible in the form of a stronger decay of the dynamic structure factor. This additional relaxation reflects the phenomenon of constraint release: the loosening of the tube confinement due to the motion of the surrounding chains.

Eventually for a short chain matrix of only one entanglement length (about 2 kg mol^{-1}) the long labelled chain displays the characteristic Rouse scaling: obviously the matrix chains are too short to confine the long chain.

The key question now is which dynamical processes underlie the CR process and lead to the gradual loss of confinement with decreasing matrix chain length. The reptation time of the matrix chains [$\tau_d(12 \text{ kg mol}^{-1}) \simeq 5000 \text{ ns}$, $\tau_d(6 \text{ kg mol}^{-1}) \simeq 500 \text{ ns}$] is far beyond the experimental time range. This holds even more for the characteristic times for constraint release $\tau_{\text{CR}} = \tau_c(M_{\text{long}}/M_e)^2$, $(M_{\text{matrix}}/M_e)^3$ (Likhtmann & McLeish, 2002) which are based on a Rouse dynamic of the tube confining the long chain. They are in the range of hundreds of microseconds. But even for the 12 kg mol^{-1} matrix, which is well entangled, the effect of CR is considerable. This fact demonstrates that for an estimation of the characteristic time-scale, all dynamical processes which are known to determine the segmental motion have to be taken into account. These processes include the reptational creep and CLF of the chain ends.

We can now design an experiment to separate the different dynamic processes (Zamponi *et al.*, 2006): For a long chain in a short matrix CLF is negligible; therefore the effect of CR of the matrix chains can be observed. On the other hand, for the dynamics of a short chain in a long matrix, the CLFs of the short chains dominate: no CR of the matrix chains can occur. Comparing the dynamic structure factor of such a pair of samples, the contribution from CLF and CR of the shorter chain can be separated. Fig. 7 shows the result for a 12 kg mol^{-1} chain in a 36 kg mol^{-1} matrix and *vice versa*. The

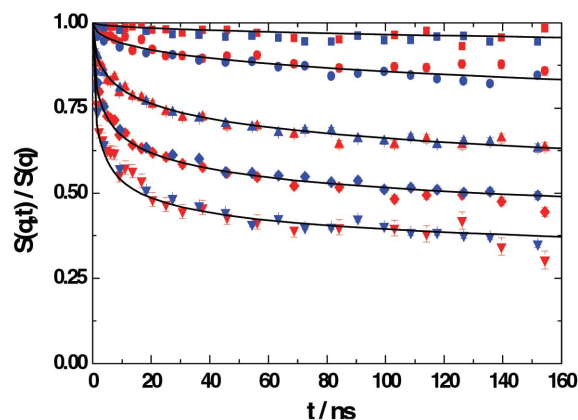


Figure 7

Dynamic structure factor of a 36 kg mol^{-1} chain in a 12 kg mol^{-1} matrix (red symbols) and *vice versa* (blue symbols). Q values (in nm^{-1}): squares 0.3 , circles 0.5 , upwards-pointing triangles 0.77 , diamonds 0.96 , and downwards-pointing triangles 1.15 . Lines are guides for the eye.

long chain relaxation by constraint release of the short matrix is obviously identical to the relaxation of the confined short chain by contour length fluctuations. That is, in the 12 kg mol^{-1} matrix the CR visible in the long chain dynamics may be traced solely to the CLF of the matrix chains. Thus, this experiment shows that even CLF alone can cause the CR effect.

4. Large-scale dynamics of biopolymers

An important endeavour for the future will be to explore to what extent the techniques we have developed for the investigation of large-scale dynamics of synthetic polymers can be transferred to biopolymers and what can we learn about the large-scale motion of such molecules. While at present the conformational dynamics on local scales have been successfully approached by *e.g.* time-dependent crystallography (Schotte *et al.*, 2003), larger-scale dynamics such as protein domain motions remain basically untouched experimentally because of the lack of techniques to study these large-scale correlated motions. Here a first NSE approach on the dynamics of *Thermus aquaticus* (*Taq*) polymerase is discussed (Bu *et al.*, 2005).

The function of DNA polymerase I from *Taq* polymerase (see Fig. 8) requires coordinated domain and subdomain motions within this protein to generate a precise ligatable nick on a DNA duplex (Lyamichev *et al.*, 1993; Kaiser *et al.*, 1999; Xu *et al.*, 2000). *Taq* polymerase performs nucleotide replacement reactions in DNA repair and RNA primer removal in DNA replication (Kornberg & Baker, 1992). During such processes, *Taq* polymerase utilizes a DNA polymerase domain to catalyze the addition of dNTP to the 3' hydroxyl terminus of an RNA primer and a 5' nuclease domain to cleave the downstream, single-stranded 5' nucleotide displaced by the growing upstream strand (Lyamichev *et al.*, 1993). Because the structure of *Taq* polymerase possesses an extended conformation with the polymerase and the 5' nuclease active sites separated by $\sim 70 \text{ \AA}$ (Kim *et al.*, 1995), the DNA needs to be shuttled between these two distant catalytic sites when switching from the DNA synthesis mode to the nucleotide cleavage mode. This scenario is similar to that which occurs when the DNA needs to be shifted from the polymerase active site to the 3'-5' exonuclease catalytic centre, which are $\simeq 30 \text{ \AA}$ apart in the Klenow fragment (the polymerase domain plus the 3'-5' exonuclease domain) domain of polymerase I, to cleave an incorrectly incorporated dNTP (Steitz, 1999). These studies imply that dynamic coupling among protein domains plays a

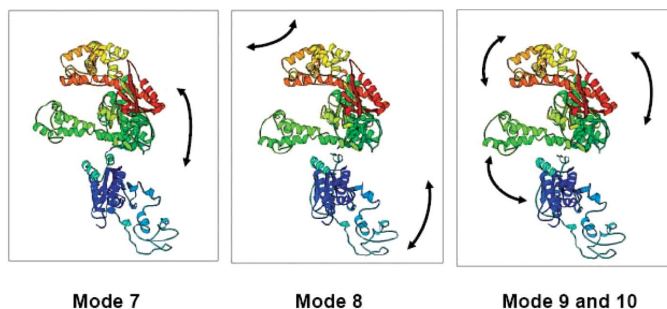


Figure 8 Structure of *Taq* polymerase and normal mode analysis (NMA). *Taq* polymerase has two distinct domains: a 5' nuclease (residues 1–289) and a KlenTaq (residues 294–831) domain connected by a linker (residues 290–305). The KlenTaq domain resembles a right hand with palm, finger and thumb subdomains. NMA on *Taq* polymerase using computer code *ELNEMO* (Suhre & Sanejouand, 2004) can identify the type and direction of internal motions. The KlenTaq domain can be subdivided into the 3'–5' exonuclease domain (residues 294–422) and the polymerase domain (residues 424–831). The first six normal modes are the translational and rotational motions of *Taq* polymerase as a whole (not shown). The lowest internal seventh and eighth normal modes are relative *en bloc* motions between the KlenTaq domain and the 5' nuclease with 5' nuclease moving towards the thumb, which is functionally important. Subdomain motions become apparent for the 9th, 10th and higher normal modes.

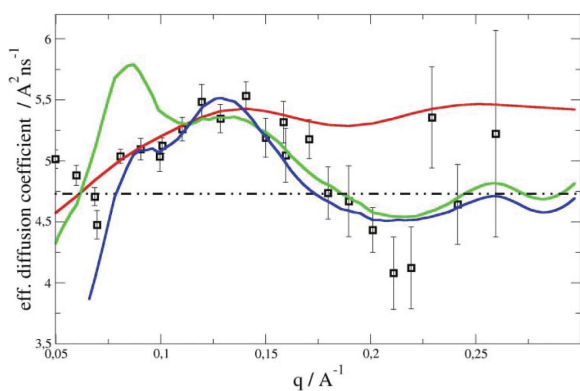


Figure 9 The figure compares the experimental $D_{\text{eff}}(Q) = \bar{\Gamma}(Q)/Q^2$ of *Taq* polymerase by NSE (open squares) with those from different dynamic models. The horizontal dashed line is $D_{t,\text{DLS}}$. The black solid line is the $D_{\text{eff}}(Q)$ of a rigid-body model of *Taq* polymerase. The red line is the $D_{\text{eff}}(Q)$ calculated using the dynamic model that parses *Taq* polymerase into two domains, the 5' nuclease and the KlenTaq domains. The blue line is the $D_{\text{eff}}(Q)$ calculated assuming three domains.

very significant (if not well appreciated) role in their biological functions.

Dilute solutions (8 mg ml⁻¹) of purified *Taq* polymerase were studied in buffered D₂O at ambient temperature. The spectra could be well fitted with single exponential decays revealing a Q -dependent relaxation rate $\bar{\Gamma}(Q)$. For a molecule performing overall translational diffusion $\bar{\Gamma}(Q) \approx Q^2$ or $D_{\text{eff}}(Q) = \bar{\Gamma}(Q)/Q^2 = \text{constant}$ would be expected. However, the effective diffusion coefficient $D_{\text{eff}}(Q)$ oscillates, as a function of Q , around the centre-of-mass translational diffusion constant measured by dynamic light scattering (DLS) ($D_{t,\text{DLS}}$) (see Fig. 9). The oscillatory behaviour of $D_{\text{eff}}(Q)$ as a function of Q indicates the presence of internal dynamics in *Taq* polymerase.

In a first step of further analysis we may convince ourselves that the oscillatory behaviour of $D_{\text{eff}}(Q)$ is not caused by the rotational diffusion of the anisotropic molecule. Using the X-ray crystal structure coordinates, the first cumulant for a rigid-body model of *Taq* polymerase was calculated. The red line in Fig. 9 displays the result,

which disagrees significantly with experimental data in the region $Q \geq 0.125 \text{ \AA}^{-1}$, suggesting that *Taq* polymerase behaves as a rigid body only on length scales longer than $2\pi/Q > 50 \text{ \AA}$. As $Q > 0.125 \text{ \AA}^{-1}$, the NSE-measured $D_{\text{eff}}(Q)$ oscillates more markedly than that calculated for the rigid-body model.

In a second step, a normal mode analysis (NMA) on *Taq* polymerase was carried out in order to identify the type and the direction of possible internal motion. In NMA, the first six modes of lowest frequency are the translational motion and rotational motion of the protein molecule as a whole. NMA suggests that the lowest frequency modes of internal motion, which are modes 7 and 8 (Fig. 8), are the *en bloc* relative motion between the 5' nuclease and the KlenTaq domains. In higher normal modes, subdomain motions appear. Specifically, in normal modes 9 and 10, the relative motions of the 5' nuclease, the 3'–5' exonuclease and the polymerase domains are apparent (see Fig. 8).

In a third step, a progression of models was created that systematically included internal normal modes by considering (i) the lowest frequency internal modes in which the 5' nuclease and the KlenTaq domains are treated as two oscillating lobes and (ii) the two lowest frequency modes that include the 5' nuclease domain but in which the KlenTaq domain is now further subdivided into its polymerase and 3'–5' exonuclease domain components. The details of this calculation are described in Bu *et al.* (2005). Case (i) is represented by the green line in Fig. 9, while the inclusion internal modes of the KlenTaq domain yields the blue line. Apparently, a systematic inclusion of higher normal modes consistently improves the agreement with the NSE experiment. Thus, the mobility tensor analysis shows that NSE data reveal coupled correlated domain motion within *Taq* polymerase. Moreover, it was shown that the internal motion can be systematically analyzed by reducing the data within a normal mode framework.

5. Conclusions and outlook

We have presented some representative results from neutron spin echo spectroscopy on the dynamics of macromolecules. In the case of linear chains we have shown that the large-scale dynamics may be well understood in terms of confinements giving rise to tube constraints as suggested by the reptation model. As the leading reptation limiting process at short time, the NSE data have quantitatively confirmed contour length fluctuations destroying the tube confinement from the ends back. Also the effect of constraint release has been observed directly on a molecular level in space and time. It has been experimentally proven that CLF of the matrix chains alone can lead to CR.

Compared to investigations of polymer dynamics, the study of the large-scale relaxational dynamics of biopolymers is still in its infancy. We have presented first experimental data on domain fluctuations in *Taq* polymerase, where it became possible to directly measure intra-protein dynamics on large scales. The data were evaluated using the most simple approach taking first cumulants which do not allow direct access to the amplitude of motions or the restoring forces. Future experiments will need to resolve the different relaxation modes separately, thereby addressing the motional amplitudes as well as possibly the forces involved. Furthermore, such experiments need to be extended to different classes of proteins where domain motion is functionally important. Maybe in the future such NSE studies will make an important contribution to a better understanding of protein function based not only on structure but also on their dynamics.

References

- Bu, Z., Biehl, R., Monkenbusch, M., Richter, D. & Callaway, J. E. (2005). *Proc. Natl Acad. Sci.* **102**, 17646–17651.
- Doi, M. & Edwards, S. F. (1978). *J. Chem. Soc. Faraday Trans.* **274**, 1789–1832.
- Doi, M. & Edwards, S. F. (1986). *The Theory of Polymer Dynamics*. Oxford: Clarendon Press.
- Gennes, P. G. de (1967). *Physics (USA)*, **3**, 37–45.
- Gennes, P. G. de (1971). *J. Chem. Phys.* **55**, 572–579.
- Gennes, P. G. de (1981). *J. Phys. (Paris)*, **42**, 735–740.
- Edwards, S. F. & Grant, J. M. V. (1973). *J. Phys. A*, **6**, 1169–1185.
- Kaiser, M. W., Lyamicheva, N., Ma, W., Miller, C., Neri, B., Fors, L. & Lyamichev, V. I. (1999). *J. Biol. Chem.* **274**, 21387–21394.
- Kim, Y., Eom, S. H., Wang, J., Lee, D. S., Suh, S. W. & Steitz, T. A. (1995). *Nature (London)*, **376**, 612–616.
- Kornberg, A. & Baker, T. A. (1992). *DNA Replication*. San Francisco: Freeman.
- Likhtman, A. E. & McLeish, T. C. B. (2002). *Macromolecules*, **35**, 6332–6343.
- Lyamichev, V., Brow, M. A. & Dahlberg, J. E. (1993). *Science*, **260**, 778–783.
- McLeish, T. C. B. (2002). *Adv. Phys.* **51**, 1379–1527.
- Mezei, F. (1980). Editor. *Neutron spin echo lecture notes in physics*, p. 128. Berlin/Heidelberg/New York: Springer.
- Richter, D., Monkenbusch, M., Arbe, A. & Colmenero, J. (2005). Editors. *Advances in Polymer Science*, p. 174. Berlin/Heidelberg/New York: Springer.
- Schleger, P., Farago, B., Lartigue, C., Kollmar, A. & Richter, D. (1998). *Phys. Rev. Lett.* **81**, 124–127.
- Schotte, F., Lim, M., Jackson, T. A., Smirnov, A. V., Soman, J., Olson, J. S., Phillips, G. N. Jr, Wulff, M. & Aninfrud, P. A. (2003). *Science*, **300**, 1944–1947.
- Steitz, T. A. (1999). *J. Biol. Chem.* **274**, 17395–17398.
- Suhre, K. & Sanejouand, Y. H. (2004). *Nucleic Acids Res.* **32**, W610–614.
- Xu, Y., Grindley, N. D. & Joyce, C. M. (2000). *J. Biol. Chem.* **275**, 20949–20955.
- Zamponi, M., Monkenbusch, M., Willner, L., Wischnewski, A., Farago, B. & Richter, D. (2005). *Europhys. Lett.* **72**, 1039–1044.
- Zamponi, M., Wischnewski, A., Monkenbusch, M., Willner, L., Richter, D., Likhtman, A. E., Kali, G. & Farago, B. (2006). *Phys. Rev Lett.* **96**, 238302 (1–4).